Journal of Applied Physics

Scrutinizing thermally stimulated current transients originating from trapped charges in organic semiconductors: A drift-diffusion study

Cite as: J. Appl. Phys. **131**, 205702 (2022); https://doi.org/10.1063/5.0088426
Submitted: 16 February 2022 • Accepted: 10 May 2022 • Published Online: 26 May 2022
Published open access through an agreement with EPFL IMX

Camilla Vael, Sandra Jenatsch, Simon Züfle, et al.

Journal of Applied Physics ARTICLE scitation.org/journal/jap

Scrutinizing thermally stimulated current transients originating from trapped charges in organic semiconductors: A drift-diffusion study

Cite as: J. Appl. Phys. **131**, 205702 (2022); doi: 10.1063/5.0088426
Submitted: 16 February 2022 · Accepted: 10 May 2022 ·
Published Online: 26 May 2022

View Online Export Citation CrossMark

Camilla Vael,[1,2] Sandra Jenatsch,[1,a)] Simon Züfle,[1] Frank Nüesch,[2,3,a)] and Beat Ruhstaller[1]

AFFILIATIONS

[1]Fluxim AG, Katharina-Sulzer-Platz 2, 8400 Winterthur, Switzerland
[2]EPFL, Institute of Materials Science and Engineering, Ecole Polytechnique Fédérale de Lausanne, Station 12, 1015 Lausanne, Switzerland
[3]Empa, Swiss Federal Laboratories for Materials Science and Technology, Laboratory for Functional Polymers, 8600 Dübendorf, Switzerland

[a)]**Authors to whom correspondence should be addressed:** sandra.jenatsch@fluxim.ch and frank.nueesch@empa.ch

ABSTRACT

Thermally stimulated current (TSC) is a widely used technique to assess trap states and extract their density, energy, and capture rate using analytical expressions. In many cases, the latter are derived from physical models pertaining to inorganic semiconductors stipulating the absence of space charge or constant lifetime of free charge carriers. Especially for organic semiconductors, the validity of these equations can, therefore, be argued. Here, we investigate the validity range of this approach by fitting the classical equations to synthetic TSC data obtained from drift-diffusion simulation using representative input parameters for organic semiconductors. We find that the equation derived for slow recapture rate as well as the initial rise method provide excellent trap parameter predictions. On the other hand, the equation using the temperature of the peak current as well as the one derived for fast retrapping have a limited range of validity. An important merit of drift-diffusion modeling is the possibility to access local variables such as charge carrier density, electric field, and recombinaton. We unravel that a small fraction of traps nearby the electrode cannot be emptied even at high temperature due to the diffusion of charge carriers from the electrode into the semiconductor. Additionally, we find that an important electrostatic factor relates the extracted charge carriers measured by the external circuit and the input trap density. For the homogeneously distributed trap states used here, this factor is precisely two. Finally, extensions of the model are analyzed by implementing temperature and field dependent mobility into the drift-diffusion model.

INTRODUCTION

Organic semiconductors (OSCs) are an intriguing class of materials with unique physical properties like high mechanical flexibility,[1] high absorption coefficient, and tunability of its optical, electronic, and dielectric characteristics.[2,3] Owing to their chemical versatility allowing to tune material properties and optimize processing, their abundance, and low cost, they are viable candidates for a broad range of applications including solar cells, light-emitting devices, transistors, diodes, and sensors.[4] By occupying a large share of the display market, organic light-emitting devices have evidenced that OSCs fully comply with the reliability requirements in this sector. Power conversion efficiency of organic photovoltaic devices is recently surging to competitive values up to 19%.[5] Although OSCs were identified as promising enablers for self-powered printed electronics, their stability and reliability still need to be further improved. Pinpointing the precise nature of degradation is a challenging task requiring the study of structural and morphological defects as well as chemical impurities.[6] Such defects always induce energetic disorder and hence produce electronic trap states impairing device performance by reducing charge carrier mobility, acting as recombination centers, changing the internal electric field distribution,[7] and reducing the effective bandgap of the material.[8–11]

Albeit difficult to identify individually, electronic trap states have a large impact on the physical and chemical properties of OSCs.

It is, therefore, possible to extract a number of parameters relevant to a particular trap distribution such as the average trap energy, energy distribution, or density. There exists a wealth of different methods to probe the characteristics of trap states. A straightforward approach consists of using electrical measurement techniques since they can also be applied to actual devices. Among others such methods include steady state or transient current–voltage measurement,[12] deep level transient spectroscopy,[13] thermal admittance spectroscopy,[14] the drain pulse method in field effect transistors,[15] impedance spectroscopy,[16] or the transient photo-voltage method,[17] which can easily be carried out as a function of temperature. Alternatively, optical methods like photothermal deflection spectroscopy (PDS)[18–20] and photoemission spectroscopy[21] may be used. It is also possible to use scanning probe methods like electric force microscopy which allows us to measure trap characteristics with a high spatial resolution.[22] In some cases, x-ray diffraction methods can be used to investigate structural defects or interface roughness.[23]

There are only a few electrical methods which measure trap states directly. One of these methods is thermally stimulated current (TSC).[24,25] In this method, deep traps are filled at low temperature either by a voltage or a light pulse. The trapped charges are subsequently released by linearly increasing the temperature and collected at the electrodes. This is a statistical process, which is controlled by a well-defined heating ramp allowing to access both thermodynamic and kinetic information. With TSC, one is, therefore, able to probe the trap energy relative to the band edge, the number of traps (or trap density), as well as the capture and release dynamics (attempt-to-escape frequency). The basic requirement is that the filled trap states at low temperature are inactive and cannot be released to the conduction states of the OSC, which are defined by the frontier orbitals of the OSC. Note that the current measured upon heating may not solely be due to released traps. Ions or reorienting dipoles as well as temperature dependent charge injection may interfere with the signal originating from trap-released charges. These effects can, however, be accounted for by recording a so-called "dark" TSC transient, where the trap filling step is omitted, and by subtracting the dark TSC transient from the actual signal. Albeit relatively easy to measure, analysis of TSC data is not straight forward since many physical factors have an influence on the shape of the TSC signal.[26] Hence, the interpretation of the measured signal relies on the application of a compact physical model allowing to fit an analytical formula to the experimental TSC data.[27] Every model, though, is subject to underlying basic assumptions, which are difficult to verify experimentally. It is, therefore, important to have a possibility for validating the models for a particular experimental system and to understand their application ranges.

In this study, we use a numerical drift-diffusion algorithm implemented in the commercial simulation software Setfos 5.1 to scrutinize the validity of the most popular analytical formula.[28] Among other input parameters, we first define the relevant trap characteristics for an OSC, which are then used to generate synthetic TSC data. We then use different analytical models to extract important trap parameters and compare the obtained values with the input parameters. We also analyze the limitations and validity range of the analytical formulas employed for TSC by varying various device, material, and experimental parameters in the simulations. This approach provides further insight in the reliability of the models and guides the experimentalist on how to design the device and optimize the measurement procedures in order to determine the trap parameters with the highest possible accuracy. Eventually, we unravel unexplored features of TSC experiments such as the correlation between extracted charges and trap density as well as the fraction of non-extractable trapped charges.

ANALYTICAL AND DRIFT-DIFFUSION MODELS

There exists a plethora of models describing TSC, which were originally developed for inorganic semiconductors.[29–31] Very often, these models originate from the phenomenon of thermally stimulated luminescence and can be directly used to describe TSC by assuming temperature independent mobility and a constant lifetime of the free carriers. For a comprehensive discussion, we refer to the book by Chen and Kirsh.[25] While these models well describe semiconductors involving discrete trap levels and constant free carrier lifetime, they may not be appropriate for disordered organic materials, where the thermally stimulated luminescence peak is observed at lower temperatures than the TSC peak.[32] Here, we focus on the most common analytical expressions initially derived for inorganic semiconductors in order to shed light on their validity range in organic semiconductors. We treat the simple case of discrete trap levels and allow for the variation of free charge carrier lifetime as well as space charge.

In a typical TSC experiment, the active material containing electronic trap states is sandwiched between two electrodes and is heated at a rate β from a start temperature T_0 to a temperature $T = T_0 + \beta^* t$, where t is the heating time. Simultaneously, the current I_{TSC} originating from released charge carriers (for the sake of simplicity, we limit ourselves to electron traps) in the material is measured by means of an appropriate extraction field. The TSC signal is characterized by a peak, which is shaped by an exponential current onset due to thermally activated carriers at early times and by a fast decline at later times related to the limited availability of filled traps. Time t and temperature T are correlated by a linear relationship such that $dt = dT/\beta$. Based on a few assumptions that will be discussed below, Haering and Adams[29] derived an analytical formula which is commonly used to describe the complete peak shape as a function of T,

$$I_{TSC} = AFe\mu\tau n_{t,0} N_0 c_n \exp\left(-\frac{E_t}{kT}\right) \exp\left[-\frac{1}{\beta}\int_{T_0}^{T} N_0(T')c_n(T')\exp\left(-\frac{E_t}{kT'}\right)dT'\right], \quad (1)$$

where A is the area of the electrode, F is the electric field, e is the elemental charge, μ is the charge carrier mobility, c_n is the electron capture coefficient, $n_{t,0}$ is the initial density of filled traps, τ is the lifetime of electrons in the transport states, N_0 is the density of transporting states, E_t is the energy difference between the transport energy level and the trap energy (trap depth), and k_B is the Boltzmann constant. Here, the capture rate coefficient c_n is used to describe trap dynamics. The latter is related to the attempt-to-escape frequency s or the capture cross section σ via $s = N_0 \nu_{th} \sigma = N_0 c$, where ν_{th} is the thermal velocity of the charge carrier. Equation (1) is valid for the special case where recombination of electrons with hole centers is dominating recapturing by the trap. In the following, we will refer to this formula as "slow" for slow retrapping.

A simplification of Eq. (1) is frequently employed, which will hereafter be referred to as the "initial rise" method. In this approximation only, the rising part of the I_{TSC} peak is considered, where temperature T_0 is close enough to the temperature of the current onset. The integral of the second exponential term in (1) is then close to zero and can, therefore, be neglected. Thus, the formula reduces to

$$I_{TSC} = AFe\mu\tau n_{t,0} N_0 c_n \exp\left(-\frac{E_t}{kT}\right). \tag{2}$$

Originally, this approach was developed by Garlick and Gibson[33] for thermally stimulated luminescence. By taking the derivative of Eq. (1) with respect to the temperature and only including the temperature dependence of c_n and N_0 explicitly after the differentiation, a simple formula for the slow retrapping case can be derived, relating the temperature at peak position T_{max} to the trap energy E_t,

$$E_t = kT_{max} \ln\left(\frac{T_{max}^4}{\beta}\right). \tag{3}$$

This formula will be referred to as "T4max" in the following. Originally, it was derived by Fang *et al.*[34] for the case of semi-insulating GaAs. Because of its simplicity, it is still widely used for the analysis of organic semiconductors and lead–halide perovskites.[35,36]

For the case where retrapping and recombination have equal probability, another expression was derived by Garlick and Gibson,[33]

$$I_{TSC} = \frac{AFe\mu\tau n_{t,0}^2 N_0 c_n \exp\left(-\frac{E_t}{kT}\right)}{N_t \left[1 + \frac{n_{t,0}}{N_t \beta} \int_{T_0}^{T} N_0(T') c_n(T') \exp\left(-\frac{E_t}{kT'}\right) dT'\right]^2}, \tag{4}$$

where N_t stands for the total density of trap states. We refer to this formula as "bimolecular" reflecting the fact that recombination depends on the product of the density of free electrons and holes. Above expressions are derived from rate equations and provide the temporal evolution of trap occupation when replacing time by temperature. Differently from Eq. (1) describing first order kinetics, Eq. (4) describes second order kinetics.

It is important to recall the basic assumptions made in the derivation of above expressions. First of all, the material is assumed to be homogeneous, allowing to correlate the density of free charge carriers to the measured current density. Furthermore, the absence of space charge and minority charge carriers as well as a constant free carrier lifetime is presumed. Finally, the effect of contacts as well as any electric field dependence is neglected. It is also assumed that at any time during heating, the number of trapped charge carriers is larger than the number of free charge carriers in conducting states ($n \ll n_t$).[37] This assumption is generally satisfied for undoped high resisitivity materials since the intrinsic number of free charge carriers is small and $n \approx n_t\, e^{-E_t/kT}$[25] (i.e., the number of free charge carriers is always significantly smaller than the number of filled trap states when $\frac{E_t}{kT} > 10$ for the whole temperature range of the experiment). Also, it is presumed that $\frac{dn}{dt} \ll \frac{dn_t}{dt}$,[30] meaning that the free charge carrier density varies slowly over time as compared to the trapped charge carrier density.

A straight forward method to extract the trap density n_t from the TSC signal is by integrating over the current peak,

$$n_t recorded = \int I_{TSC} dt \leq e n_t V, \tag{5}$$

where $n_t recorded$ is the apparent trap density and V is the volume of the sample.

Even though Eqs. (1)–(5) allow us to extract important trap parameters such as E_t, c_n, and n_t, the validity of these equations for a particular sample still has to be assessed. In particular, it is often difficult to verify experimentally that above base assumptions are fulfilled in a real device with electrical contacts. Variables such as the type of electrodes, the voltage applied or the device thickness may greatly influence the current transient of a TSC run. Also, a number of factors can lead to a reduction of the extracted charges and, therefore, to an underestimation of the traps present in the device.[38] For example, it may not be possible to fill all the traps at the start of the temperature ramp. Furthermore, recombination of charge carriers released during the TSC experiment with free charge carriers of opposite sign may depend on the applied voltage. A complementary modeling approach of TSC being able to bridge the gap between experimental parameters and the analytical approaches described above would, therefore, be highly valuable.

Drift-diffusion simulations allow us to take account of numerous experimental parameters in addition to those related to trap states. In this study, synthetic TSC data are simulated using a commercial drift-diffusion solver Setfos 5.1 by Fluxim AG[28] using representative input parameters of organic semiconductors. A typical sample for a TSC experiment consists of an organic semiconductor sandwiched between two electrodes [see Fig. 1(a)]. Even though further semiconducting layers may be applied to the device for optimizing charge extraction, we here consider the case of two metallic electrodes with variable charge injection barriers. In order to minimize charge injection from the electrodes under reverse bias condition, a small injection barrier from the anode to the highest occupied molecular orbital (HOMO) and from the cathode to the lowest unoccupied molecular orbital (LUMO) is chosen.

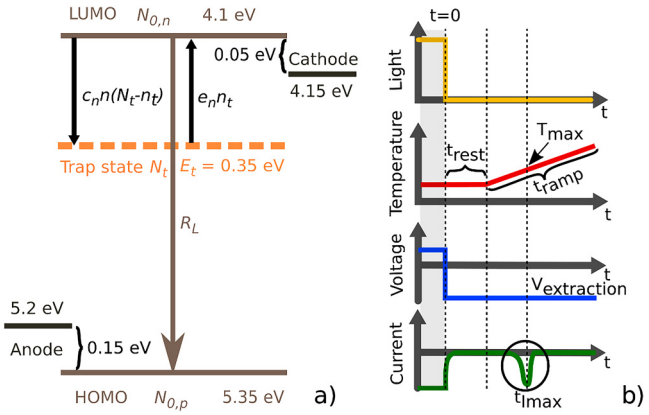

FIG. 1. (a) Simplified energy level diagram employed for this study. There are three distinct states where an electron may be found: HOMO, LUMO, or in the electron trap. $N_{0,x}$ is the density of available states for holes ($x = p$) in the HOMO or electrons ($x = n$) in the LUMO, and N_t is the total number of trap states at energy E_t. Beside extraction, there are three processes considered in the model with corresponding rate constants, namely, electron capturing (c_n), electron emission ($e_n = s_n \times \exp[E_t/kT]$), and band-to-band recombination (R_L). (b) Schematic of a TSC transient used for the generation of data by drift diffusion. $V_{extraction}$ is the employed reverse bias voltage for the extraction of detrapped charge carriers, t is the time with marked points at $t = 0$ the start of the transient simulation, t_{rest} the time where superfluous charge carriers leave the device, t_{ramp} the time during which the temperature is increased linearly, and t_{Imax} the time where the TSC peak reaches its maximum current. t_{Imax} can be converted to T_{max}, the temperature where the TSC peak reaches its maximum. Marked with the circle is the TSC signal.

In order to be able to refer to a standard device, a parameter set corresponding to typical values for amorphous organic semiconductors is defined (base case, Table S2 in the supplementary material). Trap states with an energy of 0.35 eV below the LUMO energy level are homogenously distributed in the semiconductor with a density of $N_t = 1 \times 10^{17}\,\mathrm{cm}^{-3}$. The parameters used for the stack do not correspond to one specific material but are rather average values of typical materials. For the simulations, a value for the density of states of $N_{0,p} = N_{0,n} = N_0 = 1 \times 10^{21}\,\mathrm{cm}^{-3}$ is used for both HOMO and LUMO transport levels.

The various electronic processes considered in this study are indicated in Fig. 1(a). As will be discussed below, electrons are present in the trap states before the temperature ramp of the TSC simulation starts. With increasing temperature, electrons can be emitted to the LUMO transport level at a rate e_n, from where they are either extracted at the cathode, trapped again with a capture rate c_n or undergo recombination with a hole in the HOMO level at the Langevin recombination rate R_L according to

$$R_L = \eta\gamma(np - n_i^2), \text{ with } \gamma = \frac{e(\mu_e + \mu_h)}{\varepsilon_0 \varepsilon}, \tag{6}$$

where η is the reduction factor (Langevin recombination efficiency), n is the number of free electrons, p is the number of free holes, n_i denotes the number of intrinsic charge carriers in the material, γ is the Langevin recombination constant, ϵ_0 is the vacuum permittivity, ϵ is the relative permittivity of the material, and $\mu_{e,h}$ the mobility of electrons and holes, respectively. This condition is quite different from the basic model related to Eqs. (1) and (4) since no static recombination centers are present in the drift-diffusion model and no constant lifetime can be defined. For simplicity, Shockley–Read–Hall (trap-assisted) recombination is not considered in the base case.

TSC is simulated in two steps as displayed schematically in Fig. 1(b) and corresponds to a typical experimental procedure. Traps are first filled by irradiating the sample with light (at a wavelength of 500 nm) at a temperature of 50 K (gray shaded area). The computation is carried out for the steady state at an applied forward bias of 1.05 V (flatband condition) and ensures that all of the traps are filled and the current is zero. In a second step, a transient simulation is carried out using the output of the initial steady state calculation as an initial step. There are two distinct parts in the transient simulation. During the first part, the device is kept at $T_0 = 50$ K while an extraction voltage of −2 V (reverse bias) is applied and the illumination is turned off. During this time, the superfluous charge carriers generated by the irradiation in steady state are extracted while the traps remain filled. The extracted charge carriers are recorded as a rapidly decaying current. After this equilibration step at $t = t_{rest}$, the temperature is linearly increased with a heating rate β of 10 K/min for the time $t_{ramp} = 1680$ s until it reaches 330 K. During the temperature ramp, the trapped charge carriers gain enough energy to leave the trap and are recorded as a current upon extraction. The current caused by the detrapped charges reaches a maximum at T_{max} before it declines due to the limited supply of trapped charge carriers.

In the base case drift-diffusion simulation, we consider N_0, c_n, and μ to be independent of temperature. For inorganic materials, a temperature dependence for N_0 and c_n of $T^{3/2}$ and $T^{1/2}$, respectively, is generally considered, while a temperature independent carrier mobility is adopted in advanced TSC models. According to (1), this contribution would result in a temperature dependence of T^2, which is often neglected given the fact that the exponential temperature dependence induced by the activation term clearly dominates over the power law dependence.[39,40] The same argument can be invoked for the carrier mobility in inorganic semiconductors, which also shows a power law dependence due to impurity and lattice scattering.[41] Similarly, crystalline organic semiconductors also show a linear or power law dependence of mobility with temperature, indicative of band-like transport,[42,43] which justifies the simplification of neglecting temperature dependence of above parameters in the TSC experiment. However, disordered organic semiconductors often exhibit thermally activated transport behavior where mobility increases exponentially with temperature.[44,45] Therefore, the impact of temperature dependent carrier mobility is also tackled briefly in this work (Fig. S1 in the supplementary material). Furthermore, to assess the sensitivity of trap parameter extraction on mobility, we analyze the simulated TSC curves for a large variation of electron mobilities.

RESULTS

A typical TSC simulation, hereafter called base case, is displayed in Fig. 2(a) for a 100 nm thick organic film incorporating a

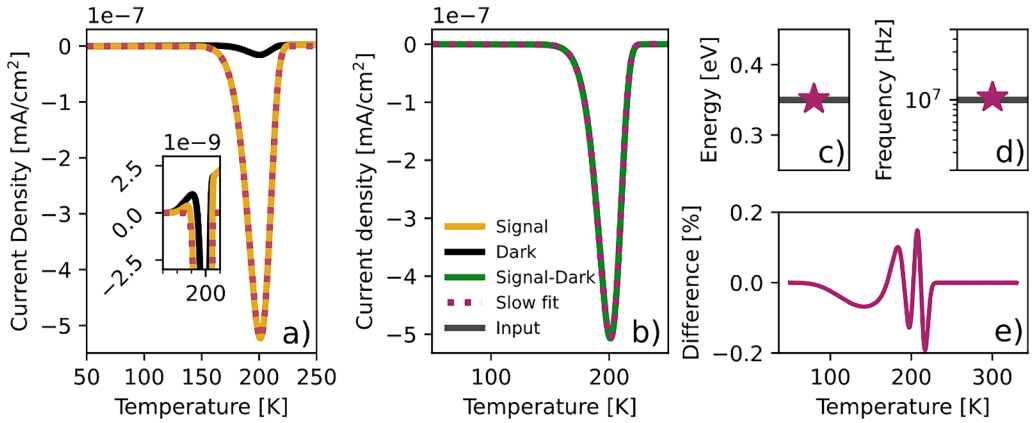

FIG. 2. (a) TSC data from drift-diffusion simulations for actual (yellow) signal and dark current (gray). For comparison, the TSC peak from Eq. (1) (slow fit, purple) is indicated. Inset: close up of the current displaying the effects of injection from the electrodes. (b) Fit using Eq. (1) (purple) to the dark current subtracted data (green). (c) and (d) Values for trap energy and attempt-to-escape frequency, respectively, extracted from the fit using Eq. (1). The gray line denotes the input value. (f) Difference in % between the dark current subtracted DD data and the full curve fit using Eq. (1).

trap density of 10^{17} cm^{-3} with an electron trap depth of 0.35 eV below the LUMO level. The device is sandwiched between two electrodes and biased at −2 V during temperature increase from 50 to 330 K at a heating rate of 10 K/min (see Tables S2–S4 in the supplementary material for all other input parameters used in the simulation). In order to simulate an actual TSC experiment and to provide synthetic TSC data for fitting to the analytical models, the dark current (where the trap filling step has been omitted) is subtracted from the TSC signal obtained with initially filled traps [Fig. 2(a)]. Interestingly, the dark current presents a clear signal contribution in addition to a small positive feature. As will be discussed below, this is due to the release of electrons from traps close to the electrode.

Fitting the analytical equations (1) and (4) to the TSC data is not trivial since I_{TSC} varies over several orders of magnitude—large values are weighted more in the least square approach used here. However, most relevant for the extraction of trap parameters is the peak itself with the largest current values. Here, we use the Levenberg–Marquardt algorithm (python library lmfit) and obtain R^2 values above 0.9998 when the extracted trap parameters match the input parameters (the goodness of the fits are above 0.998 in the other cases). The fit of the background subtracted drift-diffusion data to Eq. (1) and its residue are displayed in Figs. 2(b) and 2(f), respectively. Note that the residue is calculated as the difference between the synthetic drift-diffusion data and the curve fit using the analytical equations normalized by the maximum current value. The extracted trap energy [Fig. 2(c)] and the attempt-to-escape frequency [Fig. 2(d)] match the input values of 0.35 eV and 10^7 Hz remarkably well. Theoretically, it is also possible to calculate the trap density from the fit. However, we will refrain from it since the parameter is one factor in the product of seven other parameters, which would first need to be determined individually in other experiments. More straightforward is the integration of I_{TSC} according to (5) yielding a trap density of 4.8×10^{16} cm^{-3} which compares to about half of the input density of 10^{17} cm^{-3}.

In order to assess the accuracy of the other commonly used expressions and to probe the sensitivity of the fits to the analytical equations, a series of simulations are performed where one parameter in the base case is varied, while keeping the other parameters fixed. The extent of the change depends on the range of physically meaningful values and the range of values where the numerical calculation remains stable. Most relevant are those parameters describing the characteristics of the traps, namely, the trap energy, the trap density, and the capture rate. Also important are parameters which can easily be changed by the experimentalist such as the thickness of the semiconductor layer, the heating rate and the applied extraction voltage. The most important trap parameter is its energy, which also has the largest influence on the position of the peak. This is already visible in the analytical formulas for the TSC curve where trap energy enters as an exponent in an exponent. The extracted trap energies are presented in Fig. 3 for a range of single parameter variations, while the simulated TSC curves are shown in Fig. S3 in the supplementary material.

Figure 3(a) shows the extracted trap energy from the fits of Eqs. (1)–(4) to synthetic TSC data generated for trap energy input values of 0.1–0.55 eV. Impressively, fits with Eq. (1) yield values, which lie within 1% of the input trap energy. At low trap energies, the "initial rise" method (2) provides deviating values. This is mainly due to the fact that the TSC peak occurs close to the start temperature of the ramp. The relevant part of the peak is, therefore, not fully accessible which leads to this deviation. For trap energies of 0.2 eV and above, Eq. (2) provides the correct trap energy within an error of 5%. "T4max" equation (3) gives values for the trap energy that are close to the input value for low trap energies (<0.25 eV). However, for increasing trap energies, the extracted value starts to deviate systematically. This is an indication that the temperature dependence of the T4max formula may be stronger

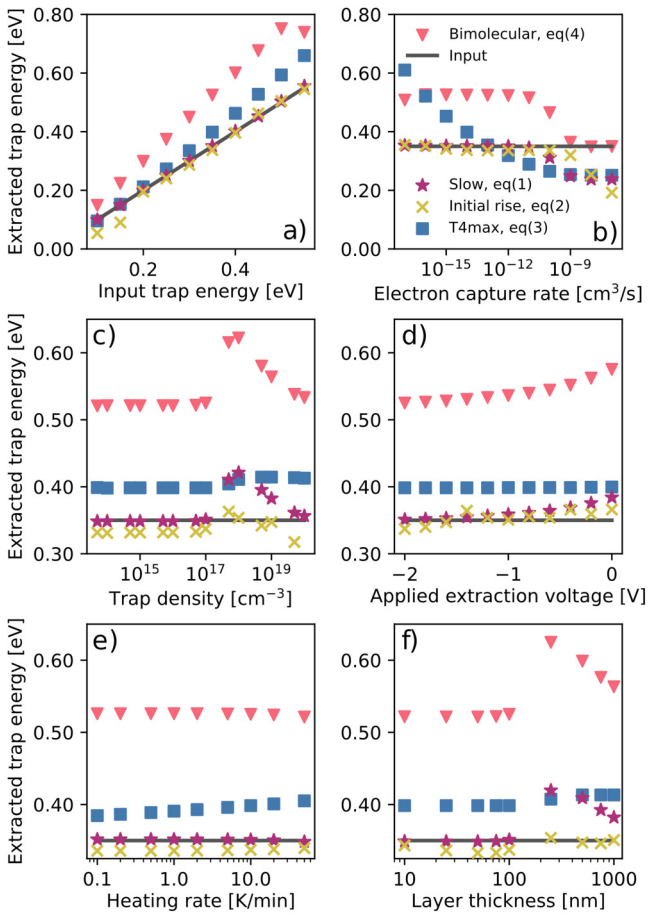

FIG. 3. Electron trap energy determined by diverse TSC formulas for different input values in single parameter variation series. The following input parameters were changed with respect to the base case: (a) trap energy, (b) capture rate, (c) trap density, (d) extraction voltage, (e) heating rate, and (f) thickness of the semiconductor film.

than the temperature dependence obtained from the drift-diffusion simulation. The "bimolecular" equation (4) does greatly overestimate the trap energy by 50% for trap energies between 0.15 and 0.5 eV. A large deviation is expected since the capture rate for the base case is in the slow retrapping regime. It is possible to measure traps with energies higher than 0.55 eV by heating the device to temperatures above 330 K. However, at such elevated temperatures, other effects such as morphological changes within the layers may occur in organic semiconductors, which can mask the effects originating from detrapping of charge carriers. We, therefore, refrained from simulating temperatures higher than 330 K.

By using a higher extraction voltage in the reverse bias, the accuracy of the extracted trap energy using (1) increases clearly [Fig. 3(d)]. The same tendency can be observed in the case of Eq. (4). However, since we are in the limit of slow retrapping, as discussed above, the trap energies are systematically too high (by 0.18 eV for an extraction voltage of −2 V). Fitting using Eq. (3) provides an energy of 0.4 eV independent of the applied extraction voltage. The values extracted using (2) are within 5% of the input trap energy with the tendency to underestimate trap energy at high extraction voltages and to overestimate it at low extraction voltages.

The range considered for the variation of the capture rate s deserves some more explanation. In the case of inorganic semiconductors, values for $s \approx 10^{11}$–10^{13} Hz are commonly used[46,47] which translates to capture rates in the range of $c_p \approx 10^{-10}$–10^{-12} cm^3 s^{-1} assuming a density of states of 10^{21} cm^{-3}. For organic semiconductors, Carr *et al.* found values ranging from 10^8 to 10^9 Hz for P3HT:PC60BM, PTB7:PC70BM, and PCDTBT:PC70BM.[40] Other studies reported values for perovskite materials of 10^9–10^{11} Hz.[48,49] However, also 5×10^{12} Hz for pentacene thin-films and 10^5 Hz for sexithiophene based transistors[50] have been reported. These numbers correspond to capture rate coefficients spanning a broad range of 1×10^{-8}–1×10^{-16} cm^3 s^{-1} assuming a density of states of 10^{21} cm^{-3}. Physically, attempt-to-escape frequency can be understood as the rate at which a trapped charge carrier interacts with molecules in its surrounding and can be estimated as a first approximation to be about an order of magnitude smaller than the relevant vibration frequency. This amounts to a capture rate of 1×10^{-14} cm^3 s^{-1} for organic materials as opposed to 1×10^{-8} cm^3 s^{-1} for inorganic materials.[25] While this accounts for the choice of the capture rate coefficient for the base case in this work, there may exist traps which are not tightly coupled to their surrounding or have a small transition probability from the trap to the LUMO. Both would lead to a lower capture rate coefficient. On the other hand, traps with high capture rate coefficients may exist. This is, for example, possible for traps that are charged when they are empty.

Capture rate variation shows a quite consistent picture. For our set of parameters, trap energies extracted for capture rates higher than 1×10^{-8} cm^{-3}/s can be described by the bimolecular formalism (4) while accurate trap energies at capture rates lower than 1×10^{-11} cm^3/s are well described using the slow retrapping rate according to Eq. (1). This is confirmed by the fits to synthetic TSC data [Fig. 3(b)]. An intermediate capture rate regime between 1×10^{-8} and 1×10^{-11} cm^3/s is indeed observed, where neither formalism will provide good values for the trap energy. Similarly to the slow retrapping formalism, Eq. (2)—which is derived from (1)—shows the same deficiencies at higher capture rates. Extraction of the trap energy from Eq. (3), however, is strongly dependent on the capture rate of the trap. Only for a value of 1×10^{-13} cm^3/s, this formula determines the trap energy with good accuracy. Indeed, the T_{max} method is free from any parameter related to trap dynamics and, therefore, cannot be used in a meaningful way without knowing the capture rate.

When looking at the influence of input trap density, Eq. (1) gives accurate values; however, for high trap densities (above 1×10^{17} cm^{-3}), an overestimation of the trap energy is found [Fig. 3(c)]. The deviation occurs due to a distortion in the peak shape [Figs. S3(d), S5(c), and S5(d) in the supplementary material], which also similarly affects the fits using Eqs. (3) and (4). Both fits, in particular Eq. (4), overestimate the trap energy systematically as discussed before. Note that Eq. (2) is rather independent of input trap density and slightly underestimates trap energy.

An important experimental parameter for TSC is the heating rate. There is a trade-off between using a high heating rate to obtain a larger signal and a low heating rate to guarantee a uniform device temperature. Our drift-diffusion model considers a constant temperature within the device and does, therefore, not allow accounting for the latter effect. All but the T_{max} method (3) show an almost constant trap energy when the heating rate is varied [Fig. 3(e)].

Film thickness too is an important experimental parameter, as thicker devices can contain more (homogeneously) distributed traps and can, therefore, lead to a larger, easier detectable current signal. Here, the film thickness is varied from 10 to 1000 nm [Fig. 3(f)]. Interestingly, Eq. (1) shows a clear deviation from the input trap energy for thicknesses larger than 100 nm. This is not the case for Eq. (2) based on the initial rise of the TSC curve. Equation (4) also shows a strong variation at larger film thicknesses. As we explain in Figs. S5(e) and S5(f) in the supplementary material, this comes from the fact that Eqs. (1) and (4) suffer from the peak shape modification due to charge transport and extraction as well as recombination, while the initial rise method [Eq. (2)] is not impacted by recombination effects due to the low concentration of detrapped holes and electrons at the onset temperature of the TSC singal.

Since the base case uses a rather low capture rate coefficient of 10^{-14} cm^3 s^{-1}, trap energies extracted from Eq. (4) derived for fast recapturing are strongly deviating from the input energy using most parameter settings in Fig. 3.

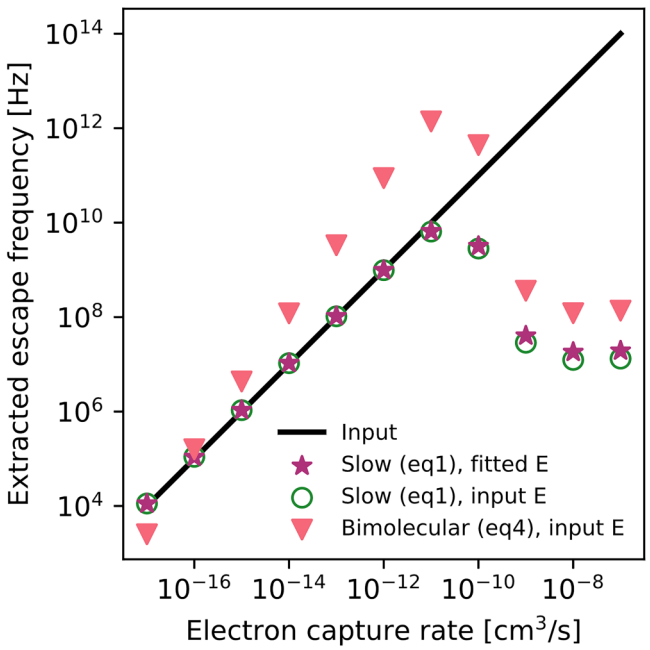

FIG. 4. Attempt-to-escape frequency s calculated from fits using Eqs. (1) and (4) for electron capture rates c_n varied from 10^{-17} to 10^{-7} cm^3/s. The trap energy was taken as an input parameter for the calculation of the attempt-to-escape frequency (triangles, circles). For comparison, the attempt-to-escape frequency was also calculated using the trap energy from the fit (stars).

It is possible to check the validity of capture rate values by generating TSC curves with different input values and extracting the capture rate. Figure 4 shows the attempt-to-escape frequency (for short: escape frequency) as a function of electron capture rate. As shown in Fig. 4, fairly accurate values for the extracted escape frequency are obtained using Eq. (1) within the limit of slow retrapping, while it is underestimated by orders of magnitude in the fast-retrapping regime. In other words, the attempt-to-escape frequency is determined with higher accuracy for all cases where also the determination of the trap energy is correct, i.e., when the assumption in the derivation of (1) are fullfilled. This finding does not change substantially when taking the input trap energy as comparted to the case where the trap energy is extracted from the fit together with the escape frequency. Using Eq. (4) for fitting, the escape frequency does not provide correct values for nearly all input electron capture rates even when the input trap energy is taken. This again highlights the shortcomings of Eq. (4) to extract decent trap parameters from the simulated data.

After analysing the reliability of the trap energy and the capture rate, we now turn our attention to the third trap parameter: the trap density. A major advantage of drift-diffusion simulations is the possibility to obtain the charge carrier density as well as the electric potential profile at each point in time during the signal. This allows us to gain more insight into the underlying processes of the TSC experiment. Here, it is used to analyze the trap distribution at different points in time and compare it to the simualtion input as well as to the calculated trap density using Eq. (5). The number of extracted charge carriers is generally expected to be smaller than the number of trap states due to incomplete trap filling or emptying and the recombination of charge carriers.

We discriminate between input trap state density N_t (100% mark), initially trapped charge carriers (gray solid line), extractable (gray dotted line) and recombined charge carriers (blue triangles), as well as recorded charge carriers which we obtain from integrating the TSC signal or the fit to it using (1) (Fig. 5). The value for extractable charges is derived from the difference of trap occupation at the start and the end of the simulation. Trap occupation is calculated at every 0.5 s and is exported every 10 s for each position in the device (0.497 nm resolution) as part of the drift-diffusion simulation. Carriers which contribute to the TSC current are obtained by integrating the dark current corrected TSC peak (green circles) and similarly for the fit using Eq. (1) (purple stars). In the base case, trap states with an energy of 0.35 eV, a homogeneous density of 10^{17} cm^{-3}, and a capture rate coefficient of 10^{-14} cm^3 s^{-1} are entirely filled at the start of the temperature ramp at $t = t_{rest}$ in the TSC experiment. Under the strong extraction field of −2 V, nearly all detrapped charge carriers will be recorded. For a homogeneous trap density, it has been shown that the recorded charge carriers correspond to $en_t/2$ (for a thorough investigation of this factor and the underlying physics refer to Hawks *et al.*[51]). For this reason, we multiply the values obtained from the integral of the TSC curve by a factor of 2 (purple plus, Fig. 5) in order to get more accurate values for the trap density. This procedure may not be accurate for an arbitrary trap distribution producing a space charge, which can drive the charges to both electrodes. Also, recombination will be

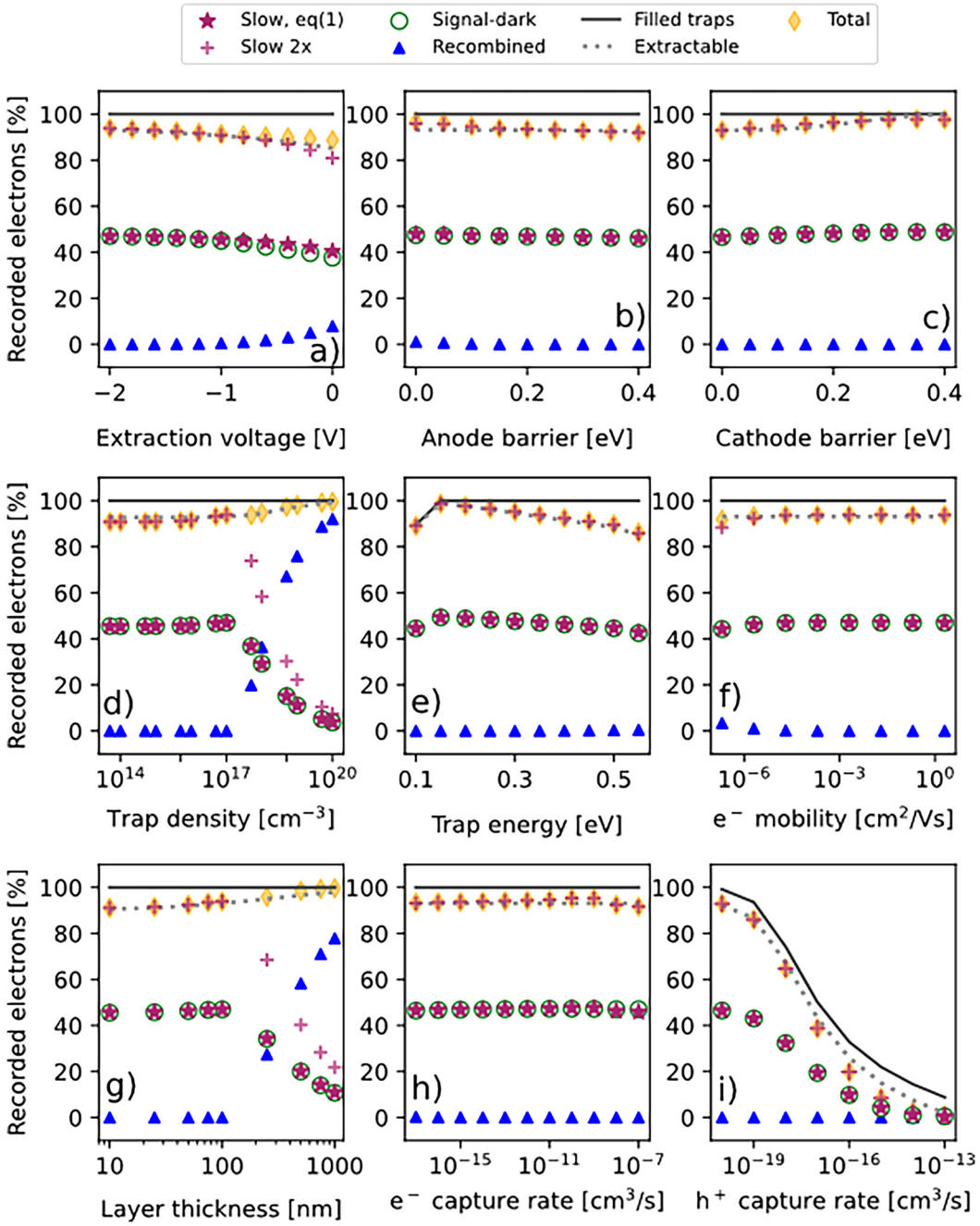

FIG. 5. Percentage of recorded electrons originating from traps as a function of a single parameter variation. The dark gray solid line indicates the fraction of filled traps at the start of the temperature ramp. The gray dotted line denotes the percentage of extractable electrons. The difference between the filled trap line and the extractable line corresponds to the percentage of electrons remaining in the electron traps at the end of the ramp. Signal-dark corresponds to the trap density in percent extracted from the simulated TSC where the dark current was subtracted. Slow fit is the trap density extracted from the integral of the fit to the signal-dark TSC curve using Eq. (1). For electronic reasons, the TSC peak attributes only $en_t/2$ of the traps. So, the values received from the integral on the fitted curve were doubled (slow ×2). The percentage of recombined charge carriers is displayed as blue triangles. The sum of slow ×2 and recombined is shown as yellow diamonds (total). Displayed are the result for following variation series: (a) extraction voltage, (b) hole injection barrier at the anode, (c) electron injection barrier at the cathode, (d) trap density, (e) trap energy relative to the LUMO, (f) electron mobility (different constant values), (g) thickness of the semiconductor layer, (h) electron capture rate, and (i) hole capture rate of the electron trap (leading to Shockley–Read–Hall recombination).

enhanced in those areas of the film where the local electric field is low. In all those cases, the number of recorded charge carriers may be considerably lower than $en_t/2$. Since there are only few free electrons other than the detrapped electrons present in the device, the recombination signal is limited by Langevin recombination of detrapped electrons with holes. This can be checked by comparing the sum of the recombined charge carriers and the recorded charge carriers (corrected by a factor of 2, "total") with the number of extractable charge carriers (see Fig. 5). If the first number is higher than the latter, charge carriers other than the detrapped electrons either recombined or were extracted.

For all parameters varied in Fig. 5, trap filling at $t = t_{rest}$ is almost always complete. A trap filling of 100% corresponds to a filled trap density of 10^{17} cm^{-3}, except in Fig. 5(d), where 100% corresponds to the respective value of the input trap density being varied in this experiment. There are two exceptions, where the fraction of filled traps is smaller than unity. The first concerns shallow traps [Fig. 5(e)], and the second considers Shockley–Read–Hall recombination [Fig. 5(i)]. A further finding is that the proportion of extractable charge carriers is generally smaller than 100%. In most cases, this proportion exceeds 90%, underlining the suitability of the TSC technique to determine the number of trap states quantitatively. For large cathode injection barriers [Fig. 5(c)], small trap energy [Fig. 5(e)], and large film thicknesses [Fig. 5(g)], the proportion of extractable charge carriers comes even close to unity. This hints to a particular effect at the cathode interface, which will be discussed below. Finally, Langevin recombination is negligible for a large range of parameters and manifests itself only for large input trap densities [Fig. 5(d)] as well as thick semiconductor layers [Fig. 5(g)].

It is interesting to analyze the prediction of trap density provided by the TSC experiment, i.e., by integrating the TSC signal and multiplying it by a factor of 2, as reasoned above (purple plus). For a very large range of parameters, the fraction of extractable charges is extremely well reproduced. Some deviation is observed for low extraction voltages [Fig. 5(a)] and very low electron mobilities [Fig. 5(f)], while substantial differences are observed for high trap densities [Fig. 5(d)] and film thicknesses above 200 nm. The latter two cases are clearly related to a high recombination of released electrons with holes in the device. These observations provide valuable input to the experimentalist in order to optimize experimental conditions and interpret the measured data adequately.

DISCUSSION

Among the various analytical expressions (1)–(4), commonly used to extract trap parameters from TSC data, Eq. (1) derived for slow retrapping clearly provides the best match to the input parameters for a large variation of input parameters. Only one parameter was varied at a time keeping the other parameters constant. For the base case, trap energy and capture rate present an excellent match (better than 0.3% for trap energy, better than 6% for capture rate), and for single parameter variations (while keeping all other parameters Table S2 in the supplementary material), a good match is obtained for the extracted trap energy (first value in bracket) and capture rate (second value in bracket) when varying the following input parameters: trap energy from 0.1 to 0.55 eV (<1%/<23% deviation), the extraction voltage from −2 to −1 V (<2.5%/<65% deviation), the capture rate from 10^{-17} to 10^{-11} cm^3 s^{-1} (<1.5%/<35% deviation), the trap density from 10^{13} to 10^{17} cm^{-3} (<0.5%/<10% deviation), the heating rate from 0.1 to 50 K min^{-1} (<0.5%/<13% deviation), and the film thickness from 10 to 100 nm (<0.5%/<9% deviation). The larger deviation for the capture rate can be attributed to (a) numerical imprecisions originating from the finite number of terms used to approach the integral in formula (1) and (b) the uncertainty from the other parameters involved in the determination of the capture rate from the fit parameter $B = \frac{N_0 c_n E_t}{\beta k_B}$, where E_t was set from the fit to the simulated data. The obtained value is usually in the same order of magnitude as the input value which is sufficiently accurate.

This excellent correspondence is not obvious given the fact that the underlying physical model of Eq. (1) only consideres conductivity and implies the absence of space charge and a constant electric field throughout the film. It is, therefore, interesting to analyze whether the latter conditions would be fulfilled in the drift-diffusion model, where space charge is naturally implemented, implying electric field variation throughout the sample. Figure 6 indicates the electron densities of free electrons and holes as well as the density of trapped electrons at the various temperatures of a TSC experiment. In the base case using an extraction voltage of −2 V [Fig. 6(a)], the high trap density of 10^{17} cm^{-3} at the start of the temperature ramp (50 K) cannot be compensated by holes. The initial space charge due to trapped electrons is gradually depleted as temperature is increased reaching a negligible level of 10^5 cm^{-3} at the end of the temperature ramp (330 K). Even though the hole density rises, it is orders of magnitude lower than the electron density throughout most of the device layer. The substantial space charge due to trapped electrons gives rise to a linearly increasing electric field, which converges to a constant field once the traps are emptied [Fig. 6(g)]. The drift-diffusion simulation, therefore, does not satisfy the hypotheses of a constant electric field or the postulated absence of space charge and minority carriers. Equation (1) also stipulates that the number of trapped charge carriers is larger than the number of free charge carriers in conducting states ($n \ll n_t$). This assumption is indeed verified throughout most of the sample thickness for tempertures where $E_t/kT > 10$. Close to the cathode, the condition is not fulfilled [Figs. 6(d) and 6(e)]. Eventually, $\frac{dn}{dt} \ll \frac{dn_t}{dt}$ is also presumed for the derivation of Eq. (1), which is fulfilled for the temperature range where the trap is active but is not yet at equilibrium with the conducting states.

The analysis of charge carrier density reveals an interesting feature close to the electrode interfaces. At the cathode, diffusion of electrons into the semiconductor inhibits emptying of traps even at high temperatures. Active electron trap states ($E_t < k_B{*}T_{max}$) are at equilibrium with free electrons in the LUMO and, thus, are partially filled. The percentage of trap occupation n_t/N_t in steady state depends on trap energy E_t, trap density N_t, temperature T, and the free electron density n as (see the supplementary material)

$$n_t/N_t = 100 \times n/[n + (N_{0,n} - n) \times \exp(-E_t/k_B T)]\,. \quad (7)$$

The density for free electrons in the LUMO close to the cathode reaches up to 1×10^{19} cm^{-3} at 330 K [Fig. 6(d)] which is

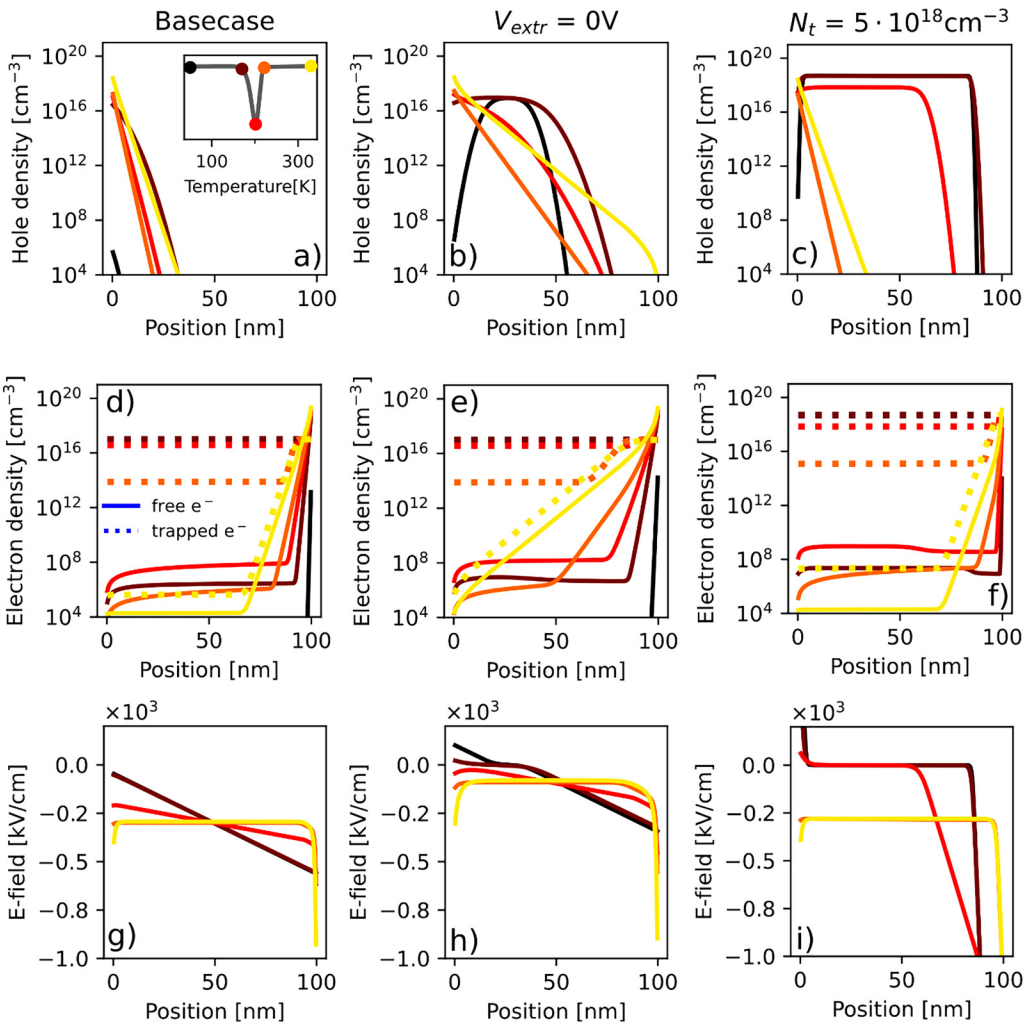

FIG. 6. Hole density (top row), electron density (middle row), and electric field (bottom row) as a function of the position inside the device for three sets of parameters at different temperatures. The anode is positioned at 0 nm, while the cathode is situated at 100 nm. (a), (d), and (g) correspond to the base case while in (b), (e), and (h), the extraction voltage V_{extr} was changed to 0 V with respect to the base case. In (c), (f), and (i), the trap density was increased to 5×10^{18} cm^{-3}. In (d)–(f), the electron densities for free (solid line) and trapped (dotted line) electrons are shown. The different colors from black (50 K, start of the TSC experiment) through to yellow (330 K, end of TSC experiment) denote the temperatures at which the electron and hole densities were extracted and correspond to the temperatures at which significant changes in the TSC curve take place [the inset in (a)]. Note: The peak maximum of the TSC occurs at different temperatures for different sets of parameters.

sufficiently high to ensure that traps in this vicinity are nearly completely filled during the whole TSC run. This explains why the fraction of extractable electrons from traps does not reach unity (see Fig. 5). At a lower extraction voltage [Fig. 6(e)], this phenomenon is even more pronounced since the free carrier density spreads over a larger width at the cathode side. For higher trap energies, the number of extractable charge carriers close to the cathode decreases, mainly caused by the increased trap occupation ratio. Increasing the thickness of the device brings the fraction of extractable trapped charges closer to unity since the cathode effect now is less important with respect to the bulk [Fig. 5(g)]. Note that the small peak in the dark current observed in Fig. 2(a) is also due to detrapping of electrons from traps close to the cathode which are filled due to diffusion from the cathode and emptied upon reaching temperatures favorable for detrapping.

The diffusion of electrons from the cathode, however, can also be reduced by employing a higher injection barrier [Fig. 5(c)]. This could indeed be a possibility to increase the number of extractable electrons. On the anode side, holes enter the semiconductor but present a small density at high extraction voltage [Fig. 6(a)]. At lower extraction voltage, however, holes can enter the device more easily and compensate trapped electrons over a large region of the

film [Fig. 6(b)] which leads to a screening of the electric field or even to an inverted field in certain regions of the device [Fig. 6(h)]. This leads to increased recombination as seen in the decrease of collected charge carriers [Fig. 5(a)]. Efficient recombination also occurs at large device thicknesses due to the small extraction fields [Fig. 5(g)]. Finally, the situation of a very high trap density (5×10^{18} cm^{-3}) is analyzed. In this case, free holes can perfectly compensate trapped electrons in the film at low temperature [Figs. 6(c) and 6(f)]. During the release of traps during heating up, electrons, therefore, easily meet a hole and recombine which drastically reduces the fraction of charge carriers extracted at the electrodes [Fig. 5(d)]. This may explain why the fit using Eq. (1) overestimates trap energy and underestimates trap density. Another factor potentially reducing the number of electrons present in traps is the trap-assisted SRH recombination (Shockley–Read–Hall recombination). During the TSC run, the number of free holes is too small for significant SRH recombination to occur. However, during the trap filling stage before the TSC run, SRH recombination may decrease the fraction of filled traps so that $n_t < N_t$. Consequently, the number of extracted electrons is smaller [Fig. 5(i)].

The initial rise method using Eq. (2) also provides excellent parameter extraction for the base case. Furthermore, this method is very stable with respect to parameter variation almost on par with Eq. (1) from where it is derived. Since only the onset of the TSC curve is used, the fitting range of the onset current is quite critical. As shown for the base case, injection of charge carriers at the onset temperature of consecutive detrapping can even lead to positive current signal [the inset in Fig. 2(a)] that may have an influence on the curve fit using Eq. (2), particularly at lower extraction fields. Moreover, the value for the trap energy extracted with the initial rise formula strongly depends on the amount of data and the part of the curve used for the fit (see Fig. S4 in the supplementary material).

As illustrated in Fig. 3(d), the initial rise method underestimates the trap energy at high extraction fields, while overestimating it at lower fields. This comes from the varying contribution of holes diffusing into the device from the anode [Fig. 6(b)]. When the activation temperature of the trapped electrons is reached, the recombination of charges sets in, reducing the current that would be expected without the presence of holes (see Fig. S5 in the supplementary material). Eventually, hole and electron currents with current peaks at different temperatures provide a net contribution to the TSC signal. Due to these combined effects, the TSC curve is distorted and T_{max} is shifted to higher temperatures, which leads to an overestimation of the trap energy.

Interestingly, the initial rise method is rather insensitive to the semiconductor thickness, while the underlying Eq. (1) shows a clear overestimation of the trap energy [Fig. 3(d)]. This is due to the fact that albeit small, the current onset will not be inhibited by the low field regions that are present through a large part of the device at the onset temperature. On the other hand, a large part of trapped charges will only be collected at higher temperatures once an appreciable electric field has been established throughout the device.

Fitting Eq. (3) to the synthetic TSC data from drift diffusion is rather problematic. For the base case, the prediction of trap energy depends very much on the power law dependence of temperature which depends ultimately on the temperature dependence of the capture rate, the density of states, and the thermal velocity of the charge carriers (see derivation of T4max formula in the supplementary material). Here, we assume all parameters to be independent of temperature, which would suggest T_{max}^2 dependence in the logarithm of Eq. (3): $E = k_B T_{max} \ln\left(\frac{T_{max}^2}{\beta}\right)$. As is shown in Fig. S2 in the supplementary material, however, the power law of T_{max}^3 provides the closest fit to the synthetic data. Also, we note that there is a huge deviation from the input trap energy upon variation of the capture rate. Therefore, the use of Eq. (3) is only meaningful if the other parameters such as the capture rate and its temperature dependence as well as the temperature dependence of the mobility and density of states have already been determined.

Extracting trap parameters from Eq. (4) shows rather large discrepancies with resepect to the input parameters used for the drift-diffusion calculation of the base case (see Figs. 3 and 4). This is indeed consistent with the underlying model, stipulating a capture rate comparable to the recombination process. In drift-diffusion simulation, the more realistic case of charge extraction plays a domint role at high extraction fields. The underlying mechanisms of the models are, therefore, radically different. One may argue that extraction may be comparable to the capture rate and, therefore, substitute for recombination in the classical model [Eq. (4)]. However, the model only provides accurate prediction of trap energy for capture rates larger than 10^{-9} cm^3 s^{-1}, which is out of range for most organic semiconductors. For these reasons, Eq. (4) should not be used to fit TSC curves obtained for organic semiconductors.

Eventually, it is interesting to verify the effect of neglecting temperature dependent charge carrier mobility since charge carrier transport by a hopping mechanism leads to an exponential temperature dependence in disordered organic semiconductors. Using an activation energy of $E_a = 0.1$ eV, TSC curves were generated and fitted to Eq. (1) [Fig. S1(a) in the supplementary material]. This did not lead to a difference between the extracted and input trap energy (difference smaller than 0.02%). Another way to probe the sensitivity of Eq. (1) is to use large variations in mobility (see Figs. S1 and S3(f) in the supplementary material). By varying the mobility from 10^{-6} to 2 cm^2 V^{-1} s^{-1}, the extracted trap energy only varied from 0.352 to 0.351 eV, demonstrating negligibly small dependence on mobility.

CONCLUSION

This study applies drift-diffusion modeling to generate TSC curves of organic semiconductors incorporating trap distributions with characteristic energy, density, and capture rate. The synthetic data revealed valuable to validate trap parameter extraction commonly obtained from analytical equations based on simple physical models. The latter assume a homogenous distribution of traps, the absence of space charge as well as a constant free carrier lifetime. Such conditions are hardly found in organic semiconductors. Advantageously, drift-diffusion simulation permits to track various local physical quantities during the TSC run. Charge carrier density of electrons and holes, carrier recombination, as well as the electric field through the device can be analyzed in detail for a large variation of parameters. This study reveals that not all

underlying hypotheses of the standard physical model are fulfilled, i.e., the absence of space charge and minority carriers or the uniformity of the electrical field throughout the sample. Despite these discrepancies, the physical model based on slow recapture rate provides remarkable parameter extraction when fitted to the synthetic drift-diffusion data. It fails, however, regarding the prediction of the charge density by a factor of two. This electrostatic factor is indeed often neglected in the analysis of TSC curves and can be straightforwardly revealed by the drift-diffusion analysis (this factor may be even larger in the case of inhomogeneous trap distributions, e.g., in the case of surface and interfacial traps). Considering this correction, the trap density is, however, well reproduced for a large range of parameter variations, e.g., for trap concentrations up to 10^{17} cm^{-3}. Furthermore, the effect of charge carrier diffusion of holes and electrons into the organic semiconductor cannot be neglected. Even at strong extraction fields and high temperatures, an appreciable density of charge carriers remains trapped and cannot be extracted. At low extraction field, this effect is even more pronounced and also allows the free charge carriers to diffuse into the device leading to recombination losses. This particular mechanism leading to non-extractable trapped charge carriers has not been discussed or quantified so far.

Regarding the equations derived from the standard model based on slow retrapping, the so-called initial rise method appears to be very robust with respect to parameter variation. It provides accurate predictions for large ranges of trap energies, densities, as well as extraction voltage and performs very well also for large sample thicknesses. Similar to the slow retrapping formula, it fails at high capture rates where the hypothesis of slow recapture rates is clearly violated. Using the simplest formula based on the temperature T_{max} of TSC peak current is generally not successful for predicting the correct trap parameters. It requires the knowledge of other trap parameters, in particular, the capture rate, which can be understood by the fact that the T_{max} method does not include trap dynamics.

Thus, drift-diffusion analysis not only allows us to understand the electronic processes taking place inside the device during a TSC run but can also provide useful information to the experimentalist in order to design samples and electrodes for a more accurate trap parameter extraction. The present approach provides a model system that can be developed further to include even more complex features. For example, exciton splitting by an external electric field could also be implemented in the case of organic semiconductors, where recombination first leads to strongly bound electron hole pairs. Above that, drift -diffusion modeling also allows us to account for non-homogeneous trap densities, trap densities including electron and hole traps or various trap energy distributions. In standard analytical approaches, such intricated situations cannot be implemented.

SUPPLEMENTARY MATERIAL

See the supplementary material for the description of the drift-diffusion model including material and device parameters used for the base case; TSC simulations using temperature dependent charge carrier mobility; derivation of the formula relating trap energy to the temperature for which maximum current in the TSC run is obtained; examples of single parameter variation of drift-diffusion data; procedure for data extraction using the initial rise method; details of the contribution of holes, electrons, and recombination of charge carriers during a TSC run; and derivation of the equilibrium concentration of trapped and free charges.

ACKNOWLEDGMENTS

This project has received funding from the European Union's Horizon 2020 Research and Innovation Programs under Grant Agreement Nos. 760949 (CORNET) and 953187 (MUSICODE).

AUTHOR DECLARATIONS

Conflict of Interest

The authors have no conflicts to disclose.

DATA AVAILABILITY

The data that support the findings of this study are available from the corresponding authors upon reasonable request.

REFERENCES

[1]S. E. Root, S. Savagatrup, A. D. Printz, D. Rodriquez, and D. J. Lipomi, Chem. Rev. **117**, 6467 (2017).
[2]A. Irfan, A. R. Chaudhary, S. Muhammad, A. G. Al-Sehemi, H. Bo, M. W. Mumtaz, and M. A. Qayyum, Results Phys. **11**, 599 (2018).
[3]X. Liu, K. S. Jeong, B. P. Williams, K. Vakhshouri, C. Guo, K. Han, E. D. Gomez, Q. Wang, and J. B. Asbury, J. Phys. Chem. B **117**, 15866 (2013).
[4]S. Ahmad, J. Polym. Eng. **34**, 279 (2014).
[5]Y. Cui, Y. Xu, H. Yao, P. Bi, L. Hong, J. Zhang, Y. Zu, T. Zhang, J. Qin, J. Ren *et al.*, Adv. Mater. **33**, 2102420 (2021).
[6]S. K. Gupta, K. Dharmalingam, L. S. Pali, S. Rastogi, A. Singh, and A. Garg, Nanomater. Energy **2**, 42 (2013).
[7]D. Ray, L. Burtone, K. Leo, and M. Riede, Phys. Rev. B **82**, 125204 (2010).
[8]H. F. Haneef, A. M. Zeidell, and O. D. Jurchescu, J. Mater. Chem. C **8**, 759 (2020).
[9]M. Mandoc, F. Kooistra, J. Hummelen, B. De Boer, and P. Blom, Appl. Phys. Lett. **91**, 263505 (2007).
[10]N. Karl, Synth. Met. **133**, 649 (2003).
[11]L. Li, G. Meller, and H. Kosina, Solid State Electron. **51**, 445 (2007).
[12]J. Dacuña and A. Salleo, Phys. Rev. B **84**, 195209 (2011).
[13]T.-P. Nguyen, C. Renaud, P. L. Rendu, and S.-H. Yang, Phys. Status Solidi **6**, 1856 (2009).
[14]S. Wang, P. Kaienburg, B. Klingebiel, D. Schillings, and T. Kirchartz, J. Phys. Chem. C **122**, 9795 (2018).
[15]H. Woo and S. Jeon, Sci. Rep. **7**, 1 (2017).
[16]L. Burtone, D. Ray, K. Leo, and M. Riede, J. Appl. Phys. **111**, 064503 (2012).
[17]Z. Lin, Sci. Rep. **10**, 12888 (2020).
[18]M. B. Upama, M. Wright, B. Puthen-Veettil, N. K. Elumalai, M. A. Mahmud, D. Wang, K. H. Chan, C. Xu, F. Haque, and A. Uddin, RSC Adv. **6**, 103899 (2016).
[19]D. Becker-Koch, B. Rivkin, F. Paulus, H. Xiang, Y. Dong, Z. Chen, A. A. Bakulin, and Y. Vaynzof, J. Phys. Condens. Matter **31**, 124001 (2019).
[20]M. Nikolka, K. Broch, J. Armitage, D. Hanifi, P. J. Nowack, D. Venkateshvaran, A. Sadhanala, J. Saska, M. Mascal, S.-H. Jung *et al.*, Nat. Commun. **10**, 2122 (2019).
[21]Y. Nakayama, S. Kera, and N. Ueno, J. Mater. Chem. C **8**, 9090 (2020).
[22]C. Große, O. Gunnarsson, P. Merino, K. Kuhnke, and K. Kern, Nano Lett. **16**, 2084 (2016).
[23]Y. Fujii, Surf. Interface Anal. **48**, 1136 (2016).

[24]P. Stallinga, *Electrical Characterization Organic Electronic Materials Devices* (John Wiley & Sons, 2009).
[25]R. Chen and Y. Kirsh, *The Analysis Thermally Stimulated Processes* (Elsevier, 1981), p. 146.
[26]A. Salleo, Org. Electron. **2013**, 341 (2013).
[27]M. Zdzislaw Szymaski and B. Luszczyska, Solution Processable Compon. Org. Electron. Devices **2019**, 483 (2019).
[28]Simulation software Setfos, version 5.1, by Fluxim AG (Switzerland), www.fluxim.com.
[29]R. R. Haering and E. N. Adams, Phys. Rev. **117**, 451 (1960).
[30]G. A. Dussel and R. H. Bube, Phys. Rev. **155**, 764 (1967).
[31]A. Lewandowski and S. McKeever, Phys. Rev. B **43**, 8163 (1991).
[32]V. Arkhipov, E. Emelianova, R. Schmechel, and H. Von Seggern, J. Non-Cryst. Solids **338**, 626 (2004).
[33]G. Garlick and A. Gibson, Proc. Phys. Soc. **60**, 574 (1948).
[34]Z. Fang, L. Shan, T. Schlesinger, and A. Milnes, Mater. Sci. Eng. B **5**, 397 (1990).
[35]P. Yu, A. Migan-Dubois, J. Alvarez, A. Darga, V. Vissac, D. Mencaraglia, Y. Zhou, and M. Krueger, J. Non-Cryst. Solids **358**, 2537 (2012).
[36]C. Qin, T. Matsushima, T. Fujihara, W. J. Potscavage, Jr., and C. Adachi, Adv. Mater. **28**, 466 (2016).
[37]A. Halperin and A. Braner, Phys. Rev. **117**, 408 (1960).
[38]A. Kadashchuk, R. Schmechel, H. Von Seggern, U. Scherf, and A. Vakhnin, J. Appl. Phys. **98**, 024101 (2005).
[39]T. Walter, R. Herberholz, C. Müller, and H. Schock, J. Appl. Phys. **80**, 4411 (1996).
[40]J. A. Carr, M. Elshobaki, and S. Chaudhary, Appl. Phys. Lett. **107**, 203302 (2015).
[41]V. K. Khanna, *Extreme Temperature Harsh-Environment Electronics* (IOP Publishing Limited, Bristol, 2017).
[42]T. Sakanoue and H. Sirringhaus, Nat. Mater. **9**, 736 (2010).
[43]W. Warta and N. Karl, Phys. Rev. B **32**, 1172 (1985).
[44]S. Heun and P. Borsenberger, Chem. Phys. **200**, 245 (1995).
[45]H. Bässler and A. Köhler, *Organic Light Emitting Diodes (OLEDs)* (Elsevier, 2013), pp. 192–234.
[46]H. Martens, P. Blom, and H. Schoo, Phys. Rev. B **61**, 7489 (2000).
[47]T. Okachi, T. Nagase, T. Kobayashi, and H. Naito, Appl. Phys. Lett. **94**, 043301 (2009).
[48]R. A. Awni, Z. Song, C. Chen, C. Li, C. Wang, M. A. Razooqi, L. Chen, X. Wang, R. J. Ellingson, J. V. Li *et al.*, Joule **4**(3), 644 (2020).
[49]V. Nandal, S. Agarwal, and P. R. Nair, arXiv:2106.06930 (2021).
[50]H. L. Gomes, P. Stallinga, F. Dinelli, M. Murgia, F. Biscarini, D. De Leeuw, T. Muck, J. Geurts, L. Molenkamp, and V. Wagner, Appl. Phys. Lett. **84**, 3184 (2004).
[51]S. A. Hawks, B. Y. Finck, and B. J. Schwartz, Phys. Rev. Appl. **3**, 044014 (2015).